Binding energy of hydrogenic impurities in polar cylindrical quantum dot

2000 J. Phys.: Condens. Matter 12 4817

(http://iopscience.iop.org/0953-8984/12/22/314)

J. Phys.: Condens. Matter **12** (2000) 4817–4827. Printed in the UK PII: S0953-8984(00)10412-6

Binding energy of hydrogenic impurities in polar cylindrical quantum dot

R Charrour†, M Bouhassoune†, M Fliyou‡, D Bria† and A Nougaoui†

† Laboratoire de Dynamique et d'Optique des Matériaux, Faculté des Sciences, Université Mohamed 1er, Oujda, Morocco

‡ Equipe de Physique du Solide, ENS BP 5206 Benssouda, Fès, Morocco

Received 16 December 1999, in final form 31 March 2000

Abstract. We have studied the polaron effect on the binding energy of shallow hydrogenic impurities in a cylindrical quantum dot using a variational approach for the finite confinement potential. The interactions of charge carriers (electron and ion) with both the confined LO phonon and surface phonons (SSO and TSO) are taken into account. The effect of these three phonon modes on the binding energy of a shallow donor is examined. The emphasis is placed on the dependence of the polaronic corrections on the quantum dot size. It is found that the correction due to the LO phonons is more important than that due to the surface optical phonon modes.

1. Introduction

In the last decade, quantum dot structures have received much attention because of their physical interest and possible advantages in optoelectronic device applications [1]. The electron–phonon interaction in such systems has been studied extensively [2–11], because the polaronic effects can strongly influence the optical and transport properties of the quantum dots. Several authors have proved the importance of the phonon modes in small semiconductor quantum dots [3, 4, 12].

Few works have dealt with the longitudinal optical phonons and the surface optical phonons in a cylindrical quantum dot. Recently, Kanyinda-Malu and de la Cruz [13] calculated the surface-mode frequencies in cylindrical dots for both cases: free-standing in vacuum and heterostructure configuration. They found that the symmetric and antisymmetric modes diverge for large values of the cylinder radius and the surface-side optical modes are radius independent in the heterostructure while they present a slight dependence on the cylinder size in the free-standing case for $R < 2$ nm. In the previous theoretical investigations of the polaronic effects in low dimensional systems, only the electron–phonon interaction was considered, not including the ion–phonon coupling. Recently, Fliyou *et al* [14] have considered this interaction for the bound polaron in spherical GaAs quantum dots; in that work the ion–phonon interaction is very weak ($\alpha_{GaAs} = 0.068$) and the ion–electron interaction via phonon exchange is ignored.

As pointed out by Marini *et al* [15] for a donor-like exciton in spherical quantum dots, this interaction affects the polaronic contribution to the binding energies where LO phonons are considered and also for the effect of an SO phonon on the binding energy of exciton in quantum well wires [16]. Here, we consider an intermediary coupling ($\alpha_{CdTe} = 0.315$). We expect that the ion–electron exchange via phonons is important and consequently the binding energy of shallow donor impurities must be modified. Following the same treatment as [17], we derive a

0953-8984/00/224817+11$30.00

confined LO phonon and two types of SO phonon mode with their eigenfrequencies in order to establish the electron (ion)–phonon interaction Hamiltonian in the framework of the dielectric continuum approximation.

The reason for the choice of the cylindrical quantum dot geometry lies in the fact that the structures of this type are relatively more convenient for fabricating devices than the others which particularly have spherical geometry. One of the major concerns in the quantum dot is the impurity state. Xia [18] has studied the donor and acceptor impurity problem in a spherical quantum dot. Vivas-Moreno and Porras-Montenegro *et al* [19] have calculated the binding energy of a shallow hydrogenic impurity located on-centre in cylindrical shape GaAs–(Ga,Al)As low-dimensional systems subjected to an axial magnetic field. In these works, the effect of the carrier–charge phonon coupling is ignored.

In this work, we report a variational calculation in the effective-mass approximation of the binding energies of shallow donor impurities in the cylindrical CdTe quantum dot embedded in a dielectric matrix. We have included the coupling effect of different phonon modes: confined LO, top mode (TSO) and side mode (SSO) with the charge carrier (electron and ion). Calculations are performed for the impurities located at the centre of the structure with a finite well depth as a function of the dot size. In section 2, we describe the theoretical model. Results and discussion are presented in section 3.

2. Calculation method

2.1. Hamiltonian

The Hamiltonian of a shallow on-centre hydrogenic impurity in a cylindrical QD, with radius R and height $H = 2d$, of CdTe embedded in dielectric matrix can be written in the effective mass approximation as follows:

$$H = H_e + H_{ph} + H_{e-ph} + H_{ion-ph}. \tag{1}$$

The electronic Hamiltonian operator H_e can be expressed as

$$H_e = -\frac{\hbar^2}{2m^*}\left[\frac{\partial^2}{\partial\rho^2} + \frac{1}{\rho}\frac{\partial}{\partial\rho} + \frac{1}{\rho^2}\frac{\partial^2}{\partial\varphi^2} + \frac{\partial^2}{\partial z^2}\right] - \frac{e^2}{\varepsilon r} + V_c(r) \tag{2}$$

where m^* is the electronic effective mass, $V_c(r)$ is the confining potential and $r = (\rho^2 + z^2)^{1/2}$ is the electron position. The dielectric constant ε is taken as the static constant ε_0 in the absence of a phonon and the optical constant ε_∞ in the presence of the phonon modes.

As the impurity is fixed at the centre of the QD, the effect of the static surface polarization energy arising from the difference in the dielectric constant between the semiconductor QD and the surrounding medium is supposed to be negligible. Our supposition is valid in the region ($H > a^*$ and $R > a^*$) where the effective mass approximation works. In the case of dot size less than a^* (strong confinement region), the dielectric mismatch will be important and must be taken into account [20].

The second term is the total Hamiltonian of the free phonon field in a cylindrical QD,

$$H_{ph} = H_{LO} + H_{TSO} + H_{SSO} \tag{3}$$

where

$$H_{LO} = \sum_{l,n_1} \hbar\omega_{LO} a^+_{ln_1} a_{ln_1} \tag{4}$$

is the Hamiltonian operator for the confined LO phonon, $a^+_{ln_1}(a_{ln_1})$ is the creation (annihilation) operator for the LO phonon of the (l, n_1)th mode with frequency ω_{LO} (they satisfy the

commutative rules for bosons) and wave vector ($k_{//} = \chi_{n_1}/R, k_z = l\pi/2d$) where χ_{n_1} is the n_1th root of the Bessel function of the zeroth order.

The Hamiltonian operators for TSO and SSO phonons are respectively:

$$H_{TSO} = \sum_{n_2,m,p} \hbar\omega_p b^+_{n_2,m,p} b_{n_2,m,p} \tag{5}$$

and

$$H_{SSO} = \sum_{n_3,m,p} \hbar\omega_{ss} B^+_{n_3,m,p} B_{n_3,m,p} \tag{6}$$

where $b^+_{\pm,n_2,m}$, $b_{\pm,n_2,m}$ and $B^+_{\pm,n_3,m}$, $B_{\pm,n_3,m}$ are respectively, the creation and annihilation operators of TSO and SSO phonons with frequency $\omega_\pm$ and ω_{ss} of the (n_2, m)th and (n_3, m)th modes. $p = +, -$ for the symmetric and anti-symmetric mode respectively.

For surface phonons the inter-subband transition can be neglected [21–23] and the electrons are assumed to occupy only the ground subband ($n = 1$, $m = 0$). We only need to consider the lowest surface phonon modes ($m = 0$) [24].

The frequencies of the different phonon modes are:

$$\omega^2_{LO} = \frac{\varepsilon_0}{\varepsilon_\infty}\omega^2_{TO} \tag{7}$$

$$\omega^2_{TSO\pm} = \frac{(\varepsilon_0 + \varepsilon_d) \mp (\varepsilon_0 - \varepsilon_d)\exp(-2q_\pm d)}{(\varepsilon_\infty + \varepsilon_d) \mp (\varepsilon_\infty - \varepsilon_d)\exp(-2q_\pm d)}\omega^2_{TO} \tag{8}$$

$$\omega^2_{SSO} = \left(1 - \frac{\varepsilon_0 + \varepsilon_\infty}{\varepsilon_\infty - \varepsilon}\right)\omega^2_{TO} \tag{9}$$

where

$$\varepsilon = -\varepsilon_d \frac{I_0(k_{n_3}R)K_1(k_{n_3}R)}{I_1(k_{n_3}R)K_0(k_{n_3}R)}. \tag{10}$$

I_0, K_0, I_1, K_1 are the modified Bessel functions of zeroth and first order, $k_{n_3} = n_3\pi/2d$ is the wave vector of the SSO phonon mode, ω_{TO} is the transverse optical-phonon frequency and ε_d is the dielectric constant of the matrix.

The corresponding TSO wave vectors ($q_{\pm,n_2}$) are the n_2th roots of the equations:

$$\pi q_{+,n_2} R J_1(q_{+,n_2}R)J_0(q_{+,n_2}R) + \exp(-2q_{+,n_2}d) - 1 = 0 \tag{11}$$

$$\pi q_{-,n_2} R J_1(q_{-,n_2}R)J_0(q_{-,n_2}R) - \exp(-2q_{-,n_2}d) - 1 = 0. \tag{12}$$

The number of wave vectors ($q_{\pm,n_2}$) is limited by the Brillouin zone condition, i.e. $q_{\pm,n_2} \leqslant \pi/2a$, where a is the lattice constant of the crystal.

The third term in equation (1) describes the Hamiltonian interaction of an electron with the different phonon modes:

$$H_{e-ph} = H_{e-LO} + H_{e-TSO} + H_{e-SSO}. \tag{13}$$

The first term is the electron–LO-phonon interaction:

$$H_{e-LO} = -\sum_{n_1} J_0\left(\chi_{n_1}\frac{\rho}{R}\right)\left[\sum_{l=1,3..} V_{ln_1}\cos\left(\frac{l\pi z}{2d}\right)(a_{ln_1} + a^+_{ln_1}) + \sum_{l=2,4..} V_{ln_1}\sin\left(\frac{l\pi z}{2d}\right)(a_{ln_1} + a^+_{ln_1})\right] \tag{14}$$

with

$$V^2_{ln_1} = \frac{1}{\Omega}\frac{4\pi e^2\hbar\omega_{LO}}{[\chi_{n_1}/R]^2 J^2_1(\chi_{n_1})[1 + [l\pi R/2d\chi_{n_1}]^2]}\left(\frac{1}{\varepsilon_\infty} - \frac{1}{\varepsilon_0}\right) \tag{15}$$

where $\Omega = 2\pi R^2 d$ is the crystal volume.

The second term in equation (13) is the electron–TSO-phonon interaction, which is given by:

$$H_{e-TSO} = -\sum_{n_2,+} V_{n_{2+}} J_0(q_{n_{2+}}\rho)\cosh(q_{n_{2+}}z)(b_{n_{2,+}} + b^+_{n_{2,+}}) - \sum_{n_2,-} V_{n_{2-}} J_0(q_{n_2} - \rho)\sinh(q_{n_{2-}}z)(b_{n_{2,-}} + b^+_{n_{2,-}}) \tag{16}$$

with

$$V^2_{n_{2,+}} = \frac{1}{S}[4\pi e^2\hbar\omega_+[1/[\varepsilon(\omega_+) - \varepsilon_0] - 1/[\varepsilon(\omega_+) - \varepsilon_\infty]]] /[q_{n_{2+}}[(\sinh(2q_{n_{2+}}d) + 2q_{n_{2+}}d)(J_1^2(q_{n_{2+}}R) - J_0(q_{n_{2+}}R)J_2(q_{n_{2+}}R)) +(\sinh(2q_{n_{2+}}d) - 2q_{n_{2+}}d)(J_0^2(q_{n_{2+}}R) + J_1^2(q_{n_{2+}}R))]] \tag{16a}$$

and

$$V^2_{n_{2,-}} = \frac{1}{S}[4\pi e^2\hbar\omega_-[1/[\varepsilon(\omega_-) - \varepsilon_0] - 1/[\varepsilon(\omega_-) - \varepsilon_\infty]]] /[q_{n_{2-}}[(\sinh(2q_{n_{2-}}d) - 2q_{n_{2-}}d)(J_1^2(q_{n_{2-}}R) - J_0(q_{n_{2-}}R)J_2(q_{n_{2-}}R)) +(\sinh(2q_{n_{2-}}d) + 2q_{n_{2-}}d)(J_0^2(q_{n_{2-}}R) + J_1^2(q_{n_{2-}}R))]] \tag{16b}$$

where

$$\varepsilon(\omega_+) = -\varepsilon_d \coth(q_{+,n_2}d) \tag{16c}$$

and

$$\varepsilon(\omega_-) = -\varepsilon_d \tanh(q_{-,n_2}d). \tag{16d}$$

The last term in equation (13) is the electron–SSO-phonon interaction

$$H_{e-SSO} = -\sum_{n_3=2,4..} \Gamma_{n_{3+}} I_0\left(\frac{n_3\pi}{2d}\rho\right)\cos\left(\frac{n_3\pi}{2d}z\right)(B_{n_{3,+}} + B^+_{n_{3,+}}) - \sum_{n_3=1,3..} \Gamma_{n_{3-}} I_0\left(\frac{n_3\pi}{2d}\rho\right)\sin\left(\frac{n_3\pi}{2d}z\right)(B_{n_{3,-}} + B^+_{n_{3,-}}) \tag{17}$$

with

$$\Gamma^2_{n_{3\pm}} = \frac{1}{S}\frac{2\pi e^2\hbar\omega_{ss}}{dk^2_{n_3}[I_0^2(k_{n_3}R) - I_0(k_{n_3}R)I_2(k_{n_3}R)]}\left(\frac{1}{\varepsilon(\omega_{ss}) - \varepsilon_0} - \frac{1}{\varepsilon(\omega_{ss}) - \varepsilon_\infty}\right) \tag{18}$$

where $S = \pi R^2$ is the cross-sectional (perpendicular to z) area of the cylindrical dot.

The last term in equation (1) is the Hamiltonian interaction of an ion with different phonon modes:

$$H_{ion-ph} = H_{ion-LO} + H_{ion-TSO} + H_{ion-SSO}. \tag{19}$$

For an ion located at the centre of a cylindrical QD, the Hamiltonian operators describing the ion–LO-phonon coupling (H_{ion-LO}), ion–TSO-phonon coupling ($H_{ion-TSO}$) and ion–SSO-phonon coupling ($H_{ion-SSO}$) can be expressed respectively as:

$$H_{ion-LO} = \sum_{n_1}\sum_{l=1,3..} V_{ln_1}(a_{ln_1} + a^+_{ln_1}) \tag{20}$$

$$H_{ion-TSO} = \sum_{n_2,+} V_{n_{2+}}(b_{n_{2,+}} + b^+_{n_{2,+}}) \tag{21}$$

$$H_{ion-SSO} = \sum_{n_3=2,4..} \Gamma_{n_{3+}}(B_{n_{3,+}} + B^+_{n_{3,+}}). \tag{22}$$

To treat the complicated Hamiltonian (1), we adopted the variational method developed by Lee *et al* [25]. The trial wave function is assumed to take the following form

$$|\psi(\rho, z)\rangle = U|0\rangle|\psi_e(\rho, z)\rangle \tag{23}$$

where $|0\rangle$, $|\psi_e\rangle$ and U are, respectively, the zero-phonon state, the electronic part and the unitary transformation operator defined as

$$U = \exp\left[\sum_{l,n_1}[f_{l,n_1}a^+_{l,n_1} - \text{cc}] + \sum_{n_2,p}[g_{n_2,p}b^+_{n_2,p} - \text{cc}] + \sum_{n_3,p}[h_{n_3,p}B^+_{n_3,p} - \text{cc}]\right]. \tag{24}$$

f_{l,n_1}, $g_{n_2,p}$ and $h_{n_3,p}$ are the functions, which are determined by the variational means.

$$\frac{\partial}{\partial f_{l,n_1}}\langle 0|U^{-1}HU|0\rangle = \frac{\partial}{\partial g_{n_2,\pm}}\langle 0|U^{-1}HU|0\rangle = \frac{\partial}{\partial h_{n_3,\pm}}\langle 0|U^{-1}HU|0\rangle = 0 \tag{25}$$

which yield the following expressions:

$$f_{ln_1} = \begin{cases} \dfrac{V_{ln_1}}{\hbar\omega_{LO}}\left(J_0\left(\chi_{n_1}\dfrac{\rho}{R}\right)\cos\left(\dfrac{l\pi}{2d}z\right) - 1\right) & \text{for odd } l \\ \dfrac{V_{ln_1}}{\hbar\omega_{LO}}J_0\left(\chi_{n_1}\dfrac{\rho}{R}\right)\sin\left(\dfrac{l\pi}{2d}z\right) & \text{for even } l \end{cases} \tag{26}$$

$$g_{n_2,+} = \frac{V_{n_2,+}}{\hbar\omega_+}(J_0(q_{n_2,+}\rho)\cosh(q_{n_2,+}z) - 1) \tag{27}$$

$$g_{n_2,-} = \frac{V_{n_2,-}}{\hbar\omega_-}J_0(q_{n_2,-}\rho)\sinh(q_{n_2,-}z) \tag{28}$$

$$h_{n_3\pm} = \begin{cases} \dfrac{\Gamma_{n_3,+}}{\hbar\omega_{ss}}\left(I_0\left(n_3\dfrac{\pi}{2d}\rho\right)\cos\left(n_3\dfrac{\pi}{2d}z\right) - 1\right) & \text{for even } n_3 \\ \dfrac{\Gamma_{n_3,-}}{\hbar\omega_{ss}}I_0\left(n_3\dfrac{\pi}{2d}\right)\sin\left(n_3\dfrac{\pi}{2d}z\right) & \text{for odd } n_3. \end{cases} \tag{29}$$

After minimizing $\langle 0|U^{-1}HU|0\rangle$ with respect to f_{l,n_1}, $g_{n_2,\pm}$ and $h_{n_3,\pm}$, we obtained the effective Hamiltonian in the atomic unit system ($a^* = \hbar^2\varepsilon_0/m^*e^2$; $R^* = m^*e^4/2\varepsilon_0^2\hbar^2$)

$$\begin{aligned} H_{eff} = &-\left[\frac{\partial^2}{\partial\rho^2} + \frac{1}{\rho}\frac{\partial}{\partial\rho} + \frac{1}{\rho^2}\frac{\partial^2}{\partial\varphi^2} + \frac{\partial^2}{\partial z^2}\right] - \frac{2}{\sqrt{\rho^2+z^2}}\frac{\varepsilon_0}{\varepsilon_\infty} + V_c(r) + V_{e-LO}(\rho, z) \\ &+V_{ion-LO} + V^{ex}_{e-LO-ion}(\rho, z) + V_{e-TSO}(\rho, z) + V_{ion-TSO} \\ &+V^{ex}_{e-TSO-ion}(\rho, z) + V_{e-SSO}(\rho, z) + V_{ion-SSO} + V^{ex}_{e-SSO-ion}(\rho, z). \end{aligned} \tag{30}$$

$V_{e-LO}(\rho, z)$, $V_{e-TSO}(\rho, z)$ and $V_{e-SSO}(\rho, z)$ are the effective potentials induced by the interaction between the electron with the confined LO phonon, the top-SO phonon and the side-SO phonon, respectively:

$$V_{e-LO}(\rho, z) = -\sum_{n_1}\frac{J_0^2((\chi_{n_1}/R)\rho)}{\hbar\omega_{LO}}\left[\sum_{l=1,3}V^2_{ln_1}\cos^2\left(\frac{l\pi}{2d}z\right) + \sum_{l=2,4}V^2_{ln_1}\sin^2\left(\frac{l\pi}{2d}z\right)\right] \tag{31}$$

$$\begin{aligned} V_{e-TSO}(\rho, z) = &-\sum_{n_2,+}\frac{V^2_{n_2,+}}{\hbar\omega_+}J_0^2(q_{n_2,+}\rho)\cosh^2(q_{n_2,+}z) \\ &-\sum_{n_2,-}\frac{V^2_{n_2,-}}{\hbar\omega_-}J_0^2(q_{n_2,-}\rho)\sinh^2(q_{n_2,-}z) \end{aligned} \tag{32}$$

$$\begin{aligned} V_{e-SSO}(\rho, z) = &-\sum_{n_3=2,4}\frac{\Gamma^2_{n_3,+}}{\hbar\omega_{ss}}I_0^2\left(n_3\frac{\pi\rho}{2d}\right)\cos^2\left(n_3\frac{\pi z}{2d}\right) \\ &-\sum_{n_3=1,3}\frac{\Gamma^2_{n_3,-}}{\hbar\omega_{ss}}I_0^2\left(n_3\frac{\pi\rho}{2d}\right)\sin^2\left(n_3\frac{\pi z}{2d}\right). \end{aligned} \tag{33}$$

The effective potentials induced by the ion–phonon (LO, TSO and SSO) coupling are expressed as:

$$V_{ion-LO} = -\sum_{n_1}\sum_{l=1,3}\frac{V_{ln_1}^2}{\hbar\omega_{LO}} \tag{34}$$

$$V_{ion-TSO} = -\sum_{n_2,+}\frac{V_{n_2,+}^2}{\hbar\omega_{+}} \tag{35}$$

$$V_{ion-SSO} = -\sum_{n_3=2,4}\frac{\Gamma_{n_3,+}^2}{\hbar\omega_{ss}}. \tag{36}$$

We define $V^{ex}_{e-LO-ion}(\rho,z)$, $V^{ex}_{e-TSO-ion}(\rho,z)$ and $V^{ex}_{e-SSO-ion}(\rho,z)$ as the electron–ion exchange potentials via an LO, TSO and SSO phonon, respectively:

$$V^{ex}_{e-LO-ion}(\rho,z) = \sum_{n_1}\sum_{l=1,3}\frac{2V_{ln_1}^2}{\hbar\omega_{LO}}J_0\left(\chi_{n_1}\frac{\rho}{R}\right)\cos\left(\frac{l\pi}{2d}z\right) \tag{37}$$

$$V^{ex}_{e-TSO-ion}(\rho,z) = \sum_{n_2,+}\frac{2V_{n_2,+}^2}{\hbar\omega_{+}}J_0(q_{n_2,+}\rho)\cosh(q_{n_2,+}z) \tag{38}$$

$$V^{ex}_{e-SSO-ion}(\rho,z) = \sum_{n_3=2,4}\frac{2\Gamma_{n_3,+}^2}{\hbar\omega_{ss}}I_0\left(n_3\frac{\pi\rho}{2d}\right)\cos\left(n_3\frac{\pi z}{2d}\right). \tag{39}$$

2.2. Ground state wave function

In the finite barrier model approximation, the potential $V_c(r)$ in the Hamiltonian (equation (2)) will be taken as zero inside the cylindrical dot ($\rho < R$ and $|z| < d$) and V_0 outside it. The corresponding ground state wave function is written as:

$$\psi_e(\rho,z) = Af(\rho)g(z)\exp(-\alpha\rho) \tag{40}$$

where A is the normalization constant. $f(\rho)$ and $g(z)$ are, respectively, the ground state solution of the Schrödinger equation in the $(x–y)$-plane and z-axis [26].

$$f(\rho) = \begin{cases} J_0\left(\theta_e\dfrac{\rho}{R}\right) & \text{if } \rho < R \\ \dfrac{J_0(\theta_e)}{K_0(\beta R)}K_0(\beta\rho) & \text{if } \rho > R \end{cases} \tag{40a}$$

with $\beta = [V_0 - (\theta_e/R)^2]^{1/2}$ and θ_e is a constant determined by the boundary condition at $\rho = R$

$$\theta_e\frac{J_1(\theta_e)}{J_0(\theta_e)} = \beta R\frac{K_1(\beta R)}{K_0(\beta R)} \tag{40b}$$

and

$$g(z) = \begin{cases} \cos\left(\pi_e\dfrac{z}{2d}\right) & \text{if } |z| < d \\ \dfrac{\cos(\pi_e/2)}{\exp(-kd)}\exp(-k|z|) & \text{if } |z| > d \end{cases} \tag{40c}$$

with $k = [V_0 - (\pi_e/2d)^2]^{1/2}$ and π_e is a constant determined by the boundary condition at $z = \pm d$

$$\tan\left(\frac{\pi_e}{2}\right) = k\frac{2d}{\pi_e}. \tag{40d}$$

2.3. Binding energy expression

In the presence of different phonon modes, the ground state energy (GSE) is obtained as:

$$E_g^{ph}(\alpha) = \langle\psi_e(\rho,z)|H_{eff}|\psi_e(\rho,z)\rangle = E_0(\alpha) + E_{e-LO}(\alpha) + E_{ion-LO} + E^{ex}_{e-LO-ion}(\alpha) + E_{e-TSO}(\alpha) + E_{ion-TSO} + E^{ex}_{e-TSO-ion}(\alpha) + E_{e-SSO}(\alpha) + E_{ion-SSO}(\alpha) + E^{ex}_{e-SSO-ion}(\alpha) \tag{41}$$

where

$$E_0(\alpha) = \left\langle \psi_e(\rho,z)\right| - \nabla_r^2 - \frac{\varepsilon_0}{\varepsilon_\infty}\frac{2}{\sqrt{\rho^2+z^2}} + V_c(r)\left|\psi_e(\rho,z)\right\rangle \tag{41a}$$

$$E_{e-LO\,(TSO,\,SSO)}(\alpha) = \langle\psi_e(\rho,z)|V_{e-LO\,(TSO,\,SSO)}(\rho,z)|\psi_e(\rho,z)\rangle \tag{41b}$$

$$E_{e-LO\,(TSO,\,SSO)-ion}(\alpha) = \langle\psi_e(\rho,z)|V^{ex}_{e-LO\,(TSO,\,SSO)-ion}(\rho,z)|\psi_e(\rho,z)\rangle. \tag{41c}$$

$E_{e-LO\,(TSO,\,SSO)}(\alpha)$, $E_{ion-LO\,(TSO,\,SSO)}$ and $E^{ex}_{e-LO\,(TSO,\,SSO)-ion}(\alpha)$ are the contribution of different phonon modes to the GSE of the bound polaron in the cylindrical quantum dot. Their expressions are so long that we cannot write them here.

We can note that the $E_{ion-LO\,(TSO,\,SSO)}$ terms are independent of the electronic state; consequently they did not contribute to the binding energy.

On the other hand, the GSE of the system without the Coulomb interaction E_{sub}^{ph} is:

$$E_{sub}^{ph} = E_{sub}^0 + E_{e-LO}(\alpha=0) + E_{ion-LO} + E^{ex}_{e-LO-ion}(\alpha=0) + E_{e-TSO}(\alpha=0) + E_{ion-TSO} + E^{ex}_{e-TSO-ion}(\alpha=0) + E_{e-SSO}(\alpha=0) + E_{ion-SSO} + E^{ex}_{e-SSO-ion}(\alpha=0) \tag{42}$$

where

$$E_{sub}^0 = \langle\psi_e(\rho,z,\alpha=0)| - \nabla_r^2 + V_c(r)|\psi_e(\rho,z,\alpha=0)\rangle. \tag{42a}$$

In the absence of the phonon modes, the GSE of the impurity donor is

$$E_g^0(\alpha) = \left\langle \psi_e(\rho,z)\right| - \nabla_r^2 - \frac{2}{\sqrt{\rho^2+z^2}} + V_c(r)\left|\psi_e(\rho,z)\right\rangle. \tag{43}$$

The impurity binding energy $E_B^{ph}(E_B^0)$ is defined as the difference of energy between the bottom of the electronic conduction band without the Coulomb interaction $E_{sub}^{ph}(E_{sub}^0)$ and the ground state energy of the impurity $E_g^{ph}(E_g^0)$ in the quantum dot:

without a phonon:

$$E_B^0 = E_{sub}^0 - \min_\alpha \lfloor E_g^0(\alpha)\rfloor \tag{44}$$

and with a phonon:

$$E_B^{ph} = E_{sub}^{ph} - \min_\alpha \lfloor E_g^{ph}(\alpha)\rfloor = E_{sub}^0 - E_0(\alpha_{min}) + \Delta E_{LO}(\alpha_{min}) + \Delta E_{TSO}(\alpha_{min}) + \Delta E_{SSO}(\alpha_{min}). \tag{45}$$

$\Delta E_{LO}(\alpha_{min})$, $\Delta E_{TSO}(\alpha_{min})$ and $\Delta E_{SSO}(\alpha_{min})$ are the polaronic corrections to the binding energy of an electron bound to an impurity in a cylindrical quantum dot.

3. Results and discussion

The present section is devoted to a discussion of numerical results obtained in the case of a CdTe microcylinder embedded in a dielectric matrix of constant $\varepsilon_d = 2.5$. The effective units of length a^* and energy R^* are: $a^* = \hbar^2\varepsilon_0/m^*e^2$; $R^* = m^*e^4/2\varepsilon_0^2\hbar^2$. The physical parameters corresponding to the polar crystal CdTe used for the numerical computation are: $m^* = 0.091\,m_0$, $\varepsilon_0 = 9.6$, $\varepsilon_\infty = 7.13$, $a^* \cong 55,91$ Å, $R^* \cong 13.34$ meV and $\hbar\omega_{LO} = 20.84$ meV. The height of the potential barrier is taken as $V_0 = 5\ R^*$.

In figure 1, the binding energies are plotted versus the cylinder radius R for different values of cylinder height ($H = 2d$). We can see that the binding energy increases as the radius decreases and reaches a maximum before the threshold R_c ($R_c = 0.26\ a^*$). At small values of $R < R_c$ discrete levels are absent in the well. The electron wave function is distributed mainly outside the cylinder. With increasing the radius of the cylinder R, the energy levels fall from the continuum spectrum into the well. On the other hand, the binding energies decline with increasing dot height H. We can conclude, as for other low dimensional structures, that the geometric confinement raises the binding energy [27]. The shape of the curves obtained in the presence of the phonon modes E_B^{ph} (dotted curves) is similar to ones obtained without phonon modes E_B^0 (solid curves). The importance of the correction due to the phonon modes is more pronounced as the hydrogenic impurity binding energy becomes larger. Indeed, for fixed H, the relative shift of this energy $\Delta E_B = E_B^{ph} - E_B^0$ reaches a maximum for the same radius as the binding energy and diminishes as well as R increases. On the other hand, this energy variation declines when the dot becomes higher along the z-direction for a given value of R. The ΔE_B behaviour leads us to conclude that the polaronic contribution is larger for dots of small dimensions. The inclusion of the ion–phonon coupling imposes an exchange

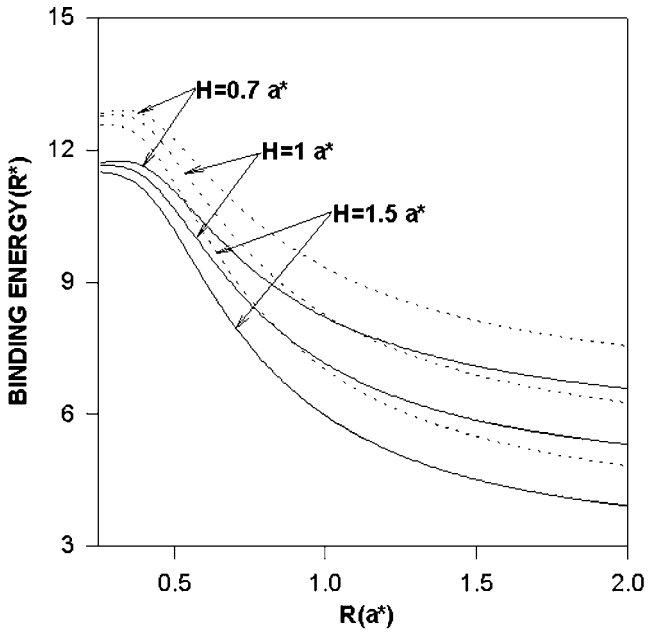

Figure 1. The variation of impurity binding energy as a function of the cylinder radius R for three values of the cylinder height ($H = 2d$). The solid and dotted curves represent the binding energies without (E_B^0) and with (E_B^{ph}) the phonon corrections, respectively.

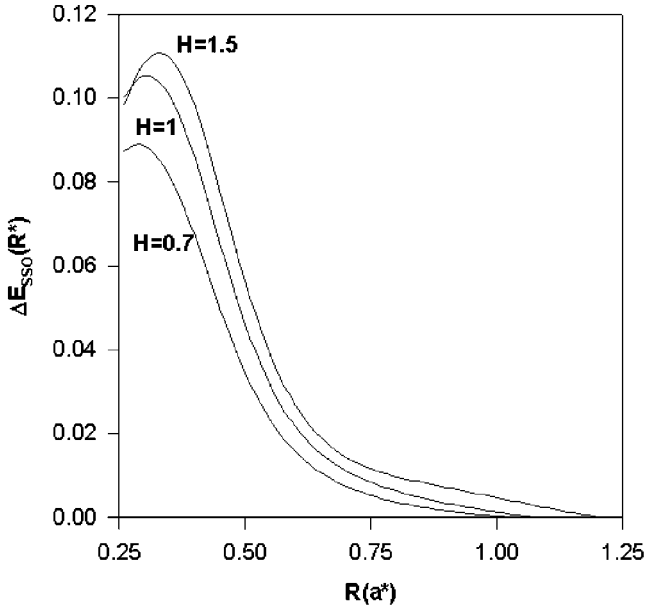

Figure 2. Polaronic correction ΔE_{SSO} to the impurity binding energy as a function of the cylindrical radius R for three values of the QD height.

term (ion–electron interaction via phonon) whose effect is substantial [15]. The contribution of each phonon modes to the binding energy has two components: one is attractive due to electron–phonon interaction and one is repulsive due to the ion–electron interaction via a phonon (exchange term). This result is in agreement with that obtained in the case of an exciton for LO and SO phonons in [15] and [16] respectively. These contributions depend on the electronic state. For the LO phonon modes, both interactions have the same behaviour as that found for the binding energy as a function of cylindrical radius for different dot heights. In addition, they are very weak near the threshold radius R_c. This is due to the small number of LO phonon modes for such a dot size. This number increases as the cylinder height augments. For a fixed value of H, the attractive interaction is higher than the exchange term in the first subband state for all cylindrical radius. However, for the impurity ground state the exchange term becomes comparable to the attractive interaction for a greater value of R. With our numerical calculation, we have remarked that this behaviour depends on the heights of the dot and the potential barrier.

Figure 2 illustrates the variation of the side surface optical phonon mode correction ΔE_{SSO} versus the cylinder radius for the same values of H as previously. We may note that this correction shows a maximum for small dot radius and vanishes rapidly as R augments. Indeed, the bound electron to the impurity feels better the effect of SSO phonon modes when it is close to the lateral surface (small width R). Furthermore, the ΔE_{SSO} rises with increasing cylinder height. The SSO phonon number grows in proportion with the increase of the dot height. Consequently, their effect on the binding energy will be important. One expects that the impact of these last modes enhances as the impurity is displaced from the centre to the lateral surface and increases when the cylinder height becomes greater by tending to the quantum well wire limit.

In figure 3, we have reported the variation of the correction introduced by the top surface optical phonon modes to the binding energy as a function of the cylinder height for different

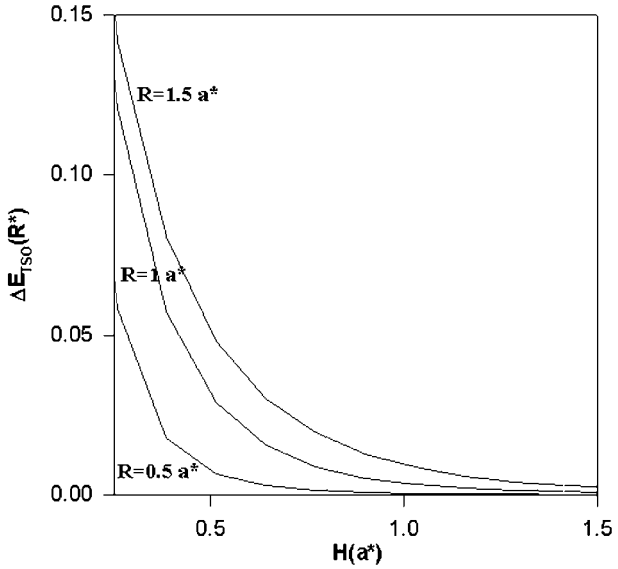

Figure 3. Polaronic correction ΔE_{TSO} to the impurity binding energy as a function of the QD height ($H = 2d$) for three values of the cylindrical radius R.

values of the QD radius R. It can be seen that the TSO modes have a prominent effect in the weak height H region. Their effect declines rapidly with the augmentation of the H dimension. In the limit of infinite dot height (quantum well wire limit) this correction vanishes.

By comparing these three corrections, we remark that the confined LO phonon mode effect is more important than the optical surface phonon ones (SSO and TSO). Consequently, the major part of the ΔE_B variation energy is due to the LO phonons.

Finally, we have to note, from our numerical calculation, that the energy exchange introduced by the ion–phonon coupling represents 33% of the polaronic correction ΔE_B.

In conclusion, we have studied the influence of the coupling between the electron and ion with both the confined phonon and the surface phonons on the binding energy of an on-centre donor impurity in a cylindrical QD embedded in a dielectric matrix. The calculations were performed within the effective-mass approximation and using a variational method. A finite deep potential describes the effect of a quantum confinement well. The result shows that the correction due to the LO phonons is more important than that of SO phonons. The side and top surface optical phonon corrections decrease rapidly as the dot size augments. Furthermore, the energy exchange between an ion and electron via phonons affects sensibly the binding energy especially for the more polar crystal. Since the charge carrier–phonon interactions are essential to understand the experimental observation of the optical absorption spectra in a semiconductor [28], we expect that the results of this work will be useful in future experiments in low-dimensional systems.

Acknowledgment

This work has been supported by the Programmes in Aid for Scientific Research (PARS) Physique 16 Oujda and Physique 03 Fès.

References

[1] Eberl K 1997 *Phys. World* **10** 47
[2] Klein M C, Hache F, Ricard D and Flytzanis C 1990 *Phys. Rev.* B **42** 11 123
[3] Zhu K D and Gu S W 1992 *Solid State Commun.* **81** 211
[4] Zhu K D and Gu S W 1992 *Solid State Commun.* **85** 651
[5] de la Cruz R M 1994 *Superlatt. Microstruct.* **16** 427
[6] Bhattacharjee A K 1995 *Phys. Rev.* B **51** 9912
[7] Wan Y, Ortiz G and Phillips P 1997 *Phys. Rev.* B **55** 5313
[8] Knipp P A, Reinecke T L, Lorke A, Fricke M and Pertroff P M 1989 *Phys. Rev.* B **56** 1516
[9] Mukhopadhyay S and Chaterjee A 1997 *Phys. Rev.* B **55** 9279
[10] Inoshita T and Sakaki H 1997 *Phys. Rev.* B **56** R4355
[11] Lépine Y and Bruneau G 1998 *J. Phys.: Condens. Matter* **10** 1495
[12] Roussignal P, Ricard D and Flytzanis C 1989 *Phys. Rev. Lett.* **62** 312
[13] Kanyinda-Malu C and de la Cruz R M 1999 *Phys. Rev.* B **59** 1621
[14] Fliyou M, Satori H and Bouayad M 1999 *Phys. Status Solidi* b **212** 97
[15] Marini J C, Stébé B and Kartheuser E 1994 *Phys. Rev.* B **50** 14 302
[16] Sheng W D and Gu S W 1993 *Solid State Commun.* **88** 111
[17] Li W S and Chen C Y 1997 *Physica* B **229** 375
[18] Xia J B 1989 *Phys. Rev.* B **40** 8500
[19] Vivas-Moreno J J and Porras-Montenegro N 1998 *Phys. Status Solidi* b **210** 723
[20] Takagahara T 1993 *Phys. Rev.* B **47** 4569
[21] Constantinou N C and Ridley B K 1990 *Phys. Rev.* B **41** 10 622
[22] Wang X F and Lei X L 1994 *Phys. Rev.* B **49** 4780
[23] Constantinou N C and Ridley B K 1989 *J. Phys.: Condens. Matter* **1** 2283
[24] Sheng W D, Xiao Y Q and Gu S W 1993 *J. Phys.: Condens. Matter* **5** L129
[25] Lee T D, Low F E and Pines D 1953 *Phys. Rev.* **90** 297
[26] Le Goff S and Stébé B 1993 *Phys. Rev.* B **47** 1383
[27] Bose C 1998 *J. Appl. Phys.* **83** 3089
Ulas M, Akbas H and Tomak M 1997 *Phys. Status Solidi* b **200** 67
[28] Devreese J T 1996 *Encyclopedia of Applied Physics* vol 14 (Weinheim: VCH) p 383